



1

2

3     **On the Role of Aerosol Radiative Effect in the Wet Season Onset Timing over the Congo**  
4                             **Rainforest during Boreal Autumn.**

5

6                     Sudip Chakraborty<sup>1\*</sup>, Jonathon H. Jiang<sup>1</sup>, Hui Su<sup>1</sup>, and Rong Fu<sup>2</sup>

7

8                     \*Corresponding author: Sudip Chakraborty. [Sudip.chakraborty@jpl.nasa.gov](mailto:Sudip.chakraborty@jpl.nasa.gov)

9

10

11             1. Jet Propulsion Laboratory, California Institute of Technology, Pasadena, CA, USA

12             2. Department of Atmospheric and Oceanic Sciences, University of California, Los  
13 Angeles

14

15

16

17

18             **Keywords:** Equatorial African Precipitation, dry season length, Wet season onset



19 **Abstract**

20 The boreal summer dry season length is reported to have been increasing in the last three decades  
21 over the Congo rainforest, which is the second-largest rainforest in the world. In some years, the  
22 wet season in boreal autumn starts early while in others it arrives late. The mechanism behind such  
23 a change in wet season onset date has not been investigated yet. Using multi-satellite datasets, we  
24 discover that the variation of aerosols in dry season plays a major role in determining the  
25 subsequent wet season onset. Dry season aerosol optical depth (AOD) influences the strength of  
26 the southern African easterly jet (AEJ-S) and thus the onset of the wet season. Higher AOD  
27 associated with a higher dust mass flux reduces the net downward shortwave radiation and  
28 decreases the surface temperature over the Congo rainforest region, leading to a stronger  
29 meridional temperature gradient between the rainforest and the Kalahari Desert as early as in June.  
30 The latter, in turn, strengthens the AEJ-S, sets in an early and a stronger easterly flow, leads to a  
31 stronger equatorward convergence and an early onset of the wet season in late August to early  
32 September. The mean AOD in the dry season over the region is strongly correlated ( $r=0.7$ ) with  
33 the timing of the subsequent wet season onset. Conversely, in low AOD years, the onset of the  
34 wet season over the Congo basin is delayed to mid-October.

35

36

37

38

39

40

41



## 42 1. Introduction

43 Wet season onset over the Congo rainforest marks the end of the dry season with increasing  
44 precipitation; thus it is important for the groundwater as well as soil moisture replenishments,  
45 photosynthetic rate, greenness, ecology, and sustainability of the rainforest, especially in a  
46 warming climate (Erfanian et al., 2017; Lewis et al., 2011, 2013; Marengo et al., 2008). Recent  
47 studies show that the Congo rainforest, which is the second-largest rainforest following the  
48 Amazon, has been experiencing a longer boreal summer dry season (Malhi and Wright, 2004;  
49 Zhou et al., 2014). The dry season length has increased by 6.4-10.4 days per decade between 1988-  
50 2013 and the rainfall is declining at a striking rate of  $-0.32 \pm 0.10$  mm/day per decade over the  
51 last 50 years (Jiang et al., 2019). Observations also indicate a long-term drying and declining of  
52 greenness in the Congo rainforest (Zhou et al., 2014). Annual rainfall over much of the Congo  
53 rainforest is marginal to sustain the rainforest (Mayer and Khalyani, 2011; Staver et al., 2011). A  
54 significant reduction of rainfall due to the delay of the main rainy season in boreal autumn can  
55 lead to significant water stress to the rainforest. Besides, continuous deforestation, droughts, and  
56 global warming pose serious threats to the rainforest, make it more vulnerable and unsustainable  
57 for future existence (Tyukavina et al., 2018).

58 Congo basin experiences two different rainy seasons during March-May (MAM) (Nicholson  
59 and Dezfuli, 2013) and September-December (SON) (Dezfuli and Nicholson, 2013) with the  
60 twice-annual passage of the intertropical convergence zone (ITCZ) (Nicholson, 2018; Nicholson  
61 and Dezfuli, 2013). The latter one (SON) during the boreal autumn is stronger, following the  
62 lengthening and widely spreading dry boreal summer (Jiang et al., 2019), and is associated with a  
63 different dynamical mechanism than that of the MAM rainy season (Jackson et al., 2009). Mid-  
64 level African Easterly jets (AEJ), especially the southern hemispheric branch (AEJ-S), are known



to play a crucial role in the boreal autumn wet season (Adebiyi and Zuidema, 2016; Jackson et al., 2009; Nicholson and Grist, 2003). The AEJ-S is associated with equatorward convergence (Adebiyi and Zuidema, 2016) and is strong during the boreal autumn season, but absent during the boreal spring or MAM season (Adebiyi and Zuidema, 2016; Jackson et al., 2009). Very intense mesoscale convective systems (MCS) are associated with the presence of the AEJ-S and bring rainfall during boreal autumn (Jackson et al., 2009; Vondou et al., 2010). Thus, the AEJ-S timing and strength might play an important role in accelerating or delaying the wet season onset over the Congo basin.

Year	Onset Pentad	Day	Month
2003	59	295	Late-October
2004	51	255	Mid-September
2005	51	255	Mid-September
2006	56	280	Early-October
2007	48	240	Late -August
2008	53	265	Late-September
2009	54	270	Late-September
2010	56	280	Early-October
2011	50	250	Early-September
2012	48	250	Early-September
Solstice	35	171	June 20
Early: 1-10; Mid: 11-20; Late: 21-31 of a month			

73

**Table 1.** Onset pentads between 2003-2012 from GPCP data.

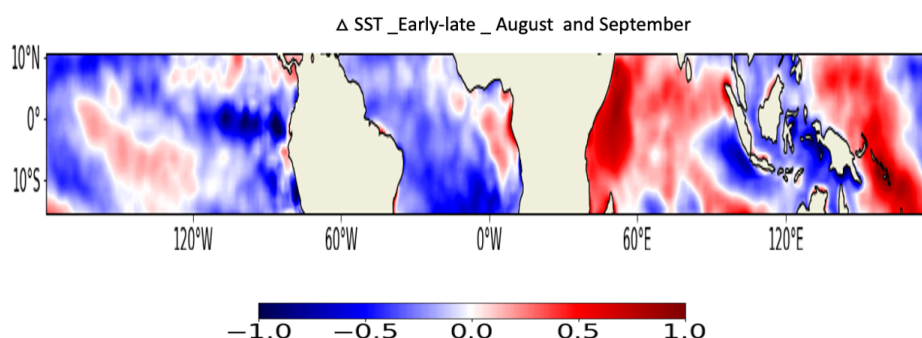
75

Out of the entire Congo basin, only the Angolan coast in the west and the eastern Zaire basin are regulated by the sea surface temperature (SST) anomalies. Circulation features associated with El Nino (La Nina) conditions are strongly linked to wet (dry) conditions over the eastern Zaire basin. Warmer western Indian Ocean SST is somewhat weakly associated with the rainfall over

79



80 there compared to a strong association between the Atlantic SST and the rainfall over the Angolan  
81 Coast (Dezfuli and Nicholson, 2013). Since rainfall onsets in the late August to early September  
82 during the early onset years (Table 1), we plot tropical  $\delta$ SST (differences in SST between early-  
83 and late-onset years and henceforth for other parameters) during August and September in Fig. 1  
84 from AIRS datasets. Fig. 1 shows that although SST over the Indian Ocean is higher, La Nina  
85 condition prevails over the Pacific Ocean during the early onset years. On the other hand, La Nina  
86 conditions, warm SST along the Benguela coast, colder western Indian Ocean are related to the  
87 wet conditions over the Angolan coast (Dezfuli and Nicholson, 2013). The rainfall variability over  
88 the Angolan coast exhibits the strongest correlation ( $r=0.74$ ) with the SST differences between the  
89 warmer Benguela current ( $10^{\circ}\text{E}$ –coast,  $2^{\circ}$ – $16^{\circ}\text{S}$ ) and colder western equatorial Indian Oceans  
90 (coast– $56^{\circ}\text{E}$ , and  $2^{\circ}$ – $14^{\circ}\text{S}$ ) (Dezfuli and Nicholson, 2013). Although La Nina condition develops  
91 and Benguela current is warmer, SST over the western equatorial Indian ocean is higher in August-  
92 September (Fig. 1) during the early onset years. As a result, SST differences between the western  
93 equatorial Indian Ocean and Benguela current decreases. Other regions over the Congo basin, such  
94 as the northern and southern areas of the Zaire basin, northern slopes of the Central African plateau,  
95 highlands of the central African Republic show weak relationships with the circulation features,  
96 sea level pressure, and SST (Dezfuli and Nicholson, 2013; Vondou et al., 2010). Rather, the rainfall  
97 variability over the central Congo basin ( $15^{\circ}$ – $25^{\circ}\text{E}$ ) is strongly associated with the stronger easterly  
98 tropical jet and local effects (Adebiyi and Zuidema, 2016; Dezfuli and Nicholson, 2013; Jackson  
99 et al., 2009; Nicholson and Grist, 2003; Vondou et al., 2010). Thus, these results explain that the  
100 SST patterns cannot solely explain the early arrival of the wet conditions over the Congo rainforest.



101

102 **Figure 1.** Map of mean of August and September  $\delta$ SST for between the early and late-onset  
 103 years.

104

105 The moisture source during the wet season is the low-level westerly jet that brings moisture from  
 106 the Atlantic Ocean below 850 hPa (Cook and Vizy, 2016; Neupane, 2016; Nicholson, 2018);  
 107 however, we observe that the difference in the atmospheric moisture content (not shown) is  
 108 insignificant between the early- and late-onset years (Dezfuli and Nicholson, 2013). Thus, over a  
 109 large part of the rainforest, as indicated by many studies in the past (Adebiyi and Zuidema, 2016;  
 110 Dezfuli and Nicholson, 2013; Jackson et al., 2009; Nicholson and Grist, 2003), zonal circulation  
 111 and stronger tropical easterly jets might explain the rainfall variability and onset timing. Hence,  
 112 we focus on the influence of the regional thermodynamic and dynamical conditions on the wet  
 113 season onset over the Congo basin as suggested by previous studies (Jackson et al., 2009; Vondou  
 114 et al., 2010).

115 On the other hand, it is known that dust aerosols are abundant with frequent outbreaks over the  
 116 Congo rainforest (Laurent et al., 2008) and they can modulate the precipitation over Africa  
 117 (N'Datchoh et al., 2018). Aerosols have a radiative cooling impact at the surface because they  
 118 reflect, scatter, and absorb sunlight (Léon et al., 2002). Such a cooling effect can influence the  
 119 meridional temperature gradient, which is the primary driver of the thermally driven jets. A few



120 attempts, mostly using model simulations, have been made to tease out the dust impacts on the  
121 west African monsoon (Lavaysse et al., 2011; Marcella and Eltahir, 2014); however, such studies  
122 over the Congo rainforest are absent. Adebisi and Zuidema (2016) found out that a high amount  
123 of aerosol concentration (aerosol optical depth, AOD>0.5) coexists with the SAE-J. However, till  
124 date, it is not clear whether aerosols can influence the wet season onset timing over the Congo  
125 rainforest despite their well-known impact on the downward shortwave radiation over the  
126 rainforest (Konzelmann et al., 1996), and the impact of the meridional temperature gradient  
127 between the Congo rainforest and the Kalahari Desert on the AEJ-S (Adebisi and Zuidema, 2016;  
128 Cook, 1999).

129 Improved understanding of the mechanisms that affect the timing of the wet season is  
130 important for an accurate representation of the wet season onset in climate models (Whittleston et  
131 al., 2017), for reducing the large uncertainty in the rainfall variability over the Congo rainforest  
132 (Whittleston et al., 2017), and assessing the future and sustainability of the rainforest under various  
133 global warming scenarios. The Congo rainforest has been far less studied compared to the Amazon  
134 rainforest (Wright et al., 2017). Although it is known that the AEJ-S is central to the boreal autumn  
135 wet season over the Congo rainforest, the reasons behind the early or late wet season onset are not  
136 clear. In particular, it is not clear whether and how aerosol loading, in addition to the  
137 meteorological, radiative, and dynamic parameters, affect the timing of the wet season onset.

138 In this study, we examine the wet season onset timing mechanism by analyzing the aerosol  
139 radiative effect on surface temperature ( $T_s$ ), AEJ-S, and associated convergence. We use a suite  
140 of satellite measurements, ERA-Interim and Modern Era Retrospective-Analysis for Research  
141 and Applications (MERRA2) dataset over 10 years (2003-2012), focusing on the domain of 5°N-  
142 10°S, 12°E-32°E to tease out the influence of the aerosol radiative effect on the wet season onset.



We analyze the differences in the above-mentioned conditions between three early-onset (2007, 2011, and 2012) and three late-onset (2003, 2006, and 2010) years (Table 1). Methods to detect the onset pentads from the Global Precipitation Climatology Project (GPCP) data are given in the methodology section. We calculate precipitation variability between the early- and late- years from GPCP data. We use cloud cover and surface irradiance data from the Cloud and the Earth's Radiant Energy System (CERES). The AOD data from the Moderate Resolution Imaging Spectroradiometer (MODIS) is used. Ts is obtained from the Atmospheric Infrared Sounder (AIRS) and ERA-interim reanalysis is used to detect the AEJ-S and calculate divergence (see Supporting Material).

## **2. Data and methodology**

### **2.1 Data**

#### **GPCP pentad data**

The Global Precipitation Climatology Project (GPCP) pentad rainfall data have been used to compute the climatological mean and the wet season onset dates. The data are provided in a 2.5° resolution at a 5 day (pentad) temporal average and available at <https://data.nodc.noaa.gov/cgi-bin/iso?id=gov.noaa.ncdc:C00933>. The version 2.2 data set has rainfall records from 1979 to present. GPCP pentad data have been used for wet season onset related analysis in previous studies (Li and Fu, 2006; Wright et al., 2017).

#### **Cloud and the Earth's Radiant Energy System (CERES)**

CERES provides cloud cover and radiant information at 1° spatial resolution at daily scale. We use the SYN1deg data set (<https://ceres.larc.nasa.gov/products.php?product=SYN1deg>) for this study. The product uses 3 hourly radiances and cloud properties to provide cloud cover, surface radiance, 500 hPa radiance values. We use the longwave and shortwave data at both the upward





as well as downward direction in the all-sky and clear-sky conditions. CERES data have previously been used in wet season onset related studies (Wright et al., 2017) are well-validated against the in-situ measurements (Loeb et al., 2018).

### **Moderate Resolution Imaging Spectroradiometer (MODIS)**

We use MODIS daily aerosol products to calculate daily aerosol optical depth (AOD) over the domain. MODIS provides AOD over the oceans and land at a spatial resolution of 10 x 10, 1 km pixels by using the deep blue algorithm. The MODIS onboard the Aqua satellite data are available every day from 2002 (<https://ladsweb.modaps.eosdis.nasa.gov/missions-and-measurements/science-domain/aerosol>) and have been extensively used for scientific purposes in the past few decades (Adebiyi and Zuidema, 2016; Fan et al., 2016).

### **Atmospheric Infrared Sounder (AIRS)**

AIRS data are available from 08-21-2002 ([https://disc.gsfc.nasa.gov/datasets/AIRX3STD\\_006/summary?keywords=airs%20version%206](https://disc.gsfc.nasa.gov/datasets/AIRX3STD_006/summary?keywords=airs%20version%206)) with a spatial coverage of 180°E to 180°W and 90°S to 90°N. We use the AIRS in combination with Advanced Microwave Sounding Unit (AMSU) and the Humidity Sounder for Brazil (HSB) data. These data use visible, infrared, and microwave sensors to estimate water vapor and 2m surface temperature. AIRS is an instrument onboard the Aqua satellite, which is a part of the A-Train constellation. We use the AIRX3STD (Susskind et al., 2014) daily version 6 standard physical retrieval data at 1° horizontal resolution.

### **ERA-Interim**

We use ERAi data that are available from 1979 to August 2019. We use the zonal and meridional wind data to analyze the wind field and the jet location for our study. Previous studies have already used ERAi data to detect the African jets (Cook, 1999; Jackson et al., 2009). The data are



189 available at a  $0.75 \times 0.67$  spatial resolution in the longitudinal and latitudinal direction,  
190 respectively at four different hours (00, 06, 12, 18) of temporal resolution. The data are available  
191 at 60 pressure levels from the surface to 0.1 hPa, which can be found at  
192 <https://www.ecmwf.int/en/forecasts/documentation-and-support/60-model-levels>. We have used  
193 673 hPa and 897 hPa levels wind data to calculate the intensity and direction of the Southern as  
194 well as Northern African Easterly jets (AEJ-S and AEJ-N) and low level African westerly jet,  
195 respectively.

## 196 **Modern Era Retrospective-Analysis for Research and Applications (MERRA2)**

197 We use two-dimensional hourly averaged surface and vertically integrated aerosol mass fluxes  
198 ( $\text{tavg1\_2d\_aer\_Nx}$ ) from the Modern Era Retrospective-Analysis for Research and Applications  
199 (MERRA2) dataset (Gelaro et al., 2017). The gridded data are provided in 576 grids along the  
200 longitudinal and 361 grids along the latitudinal direction. The data provide five different aerosol  
201 mass fluxes, such as dust (DU), organic carbon (OC), black carbon (BC), sulfates (SU), and sea  
202 salt (SS) in the zonal and meridional direction. We use this dataset to estimate the dominant  
203 aerosol types that contribute to the largest fraction to the aerosol concentrations. The MERRA-2  
204 aerosol reanalysis data are validated against 793 Aerosol Robotic Network (AERONET) stations  
205 (Gueymard and Yang, 2020) and has already been used for scientific purposes (Sitnov et al.,  
206 2020; Xu et al., 2020).

## 207 **2.2 Methods**

208 We first compute mean rainfall over the domain ( $5^{\circ}\text{N}$ - $10^{\circ}\text{S}$ ,  $12^{\circ}\text{E}$ - $32^{\circ}\text{E}$ ) from 1979 for each pentad.  
209 GPCP Pentad data have often been used to detect wet season onset over other regions of the world  
210 (Li and Fu, 2006; Wright et al., 2017). The climatological (1979-2013) mean rainfall is 4.14  
211 mm/day over the domain. We detect onset dates each year based on three criteria: 1) the rainfall



212 of that pentad is higher than the climatological mean, 2) five out of eight pentads before that pentad  
 213 has rainfall less than the climatological mean, and 3) five out of eight pentads after that pentad has  
 214 rainfall more than the climatological mean (Wright et al., 2017). Onset pentads between 2003-  
 215 2012 are shown in Table 1. We used GPCP daily data to compute five days (pentad) rainfall. We  
 216 compute rainfall time series during the three early (2007, 2011, 2012) and three late (2003, 2006,  
 217 2010) in Fig. 1A. The differences in rainfall and other parameters including cloud cover, AOD,  
 218 wind speed of the AEJ-S, and radiation fluxes from June to September between the early- and late-  
 219 onset years are computed.

220 We compute cloud cover from CERES and AOD from MODIS datasets. We compute  
 221 pentad values of low, mid-low, mid-high, and high cloud cover (%) over the domain. To  
 222 compute AOD, we used daily Aqua MODIS AOD data and averaged over five consecutive days  
 223 to estimate pentad AOD values over the domain. To understand the relationships between  
 224 rainfall onset and meteorological as well as dynamical conditions over the domain, we have  
 225 computed various other parameters from various satellites and ERA-interim reanalysis datasets.  
 226 We compute net downward shortwave energy (SWnet) as a difference between the downward  
 227 shortwave energy and upward shortwave energy at the surface from CERES data.

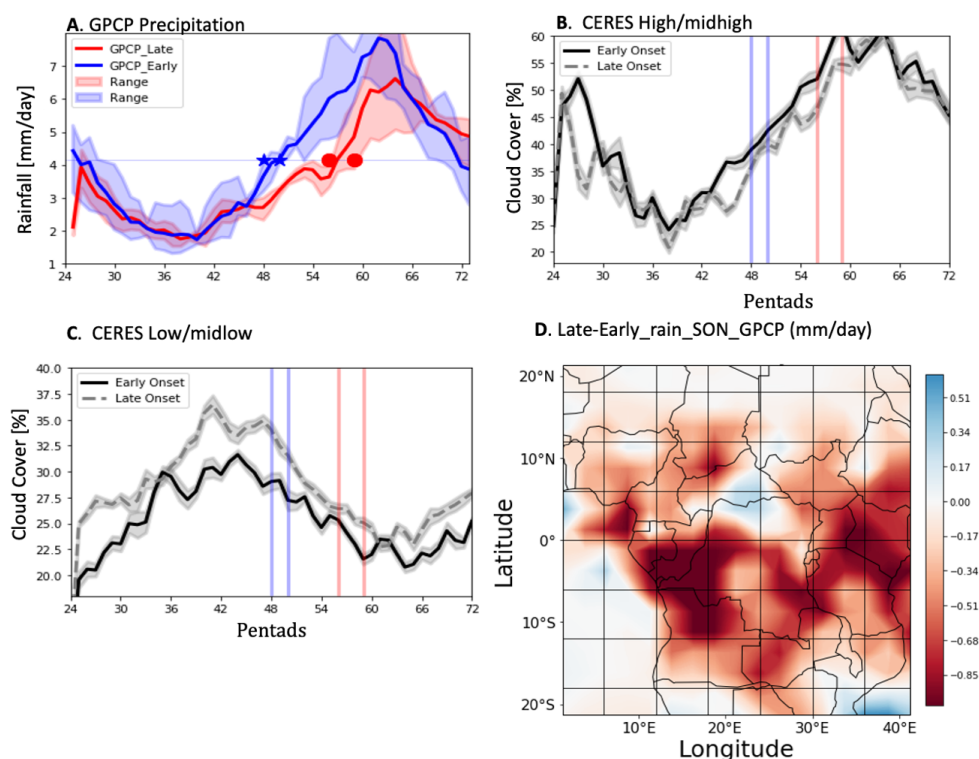
228 We use daily AIRS 2m surface temperature (Ts) to calculate the pentad values over the  
 229 domain. To detect the African Easterly Jets, we use ERA interim zonal and meridional wind  
 230 data. For the Southern African Easterly Jet (AEJ-S), we use the 650 hPa between 5°-15°S and  
 231 12°-24° E (Adebiyi and Zuidema, 2016). We show the wind map of the jet over the domain in  
 232 Figure 3. We also use wind speed and direction in our analysis to show the maps of the easterly  
 233 jets at 650 hPa. To compute divergence, we have used the divergence equation as:

234 
$$div = \frac{du}{dx} + \frac{dv}{dy}$$



Where  $u$  and  $v$  are the zonal and meridional wind and  $x$  and  $y$  are the longitudinal and latitudinal distances, respectively.

### 3. Results



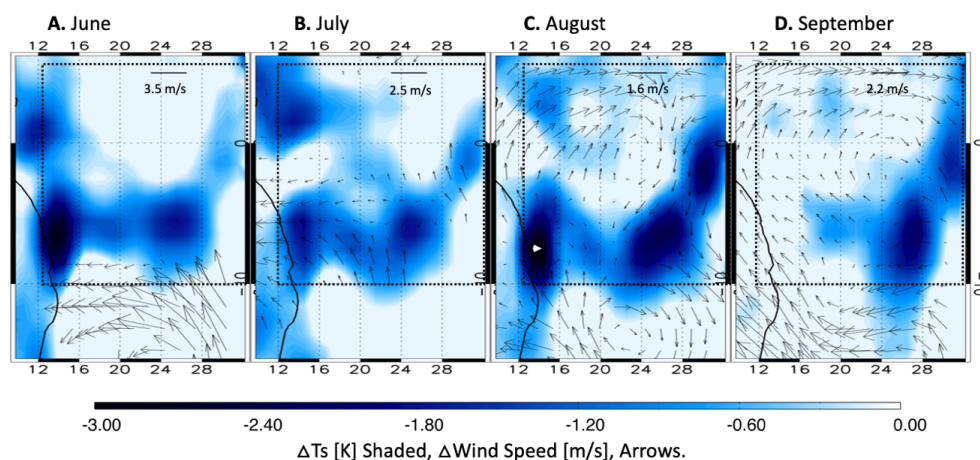
**Figure 2.** (A) Mean precipitation time series during the early (blue) and late (red) onset years at each pentad. Blue stars (red circles) represent the timing of the early (late) onset years. Rainfall ranges represent precipitation of individual late- or late-onset years. Mean high and mid-high cloud cover (B) and low and mid-low cloud cover (C) during the early and late-onset years. Vertical lines show the ranges of onset times during the early (blue) and late (red) years. (D) Maps of precipitation differences between the late and early-onset years using GPCP data.

Figure 2A shows a time series of precipitation over the domain during the early and late-onset years. Precipitation (Fig. 2A) and high cloud cover (Fig. 2B) increases during August (42–48<sup>th</sup> pentads) when the wet season is early (blue stars, Fig. 2A) compared to their slower pick-up during the late-onset years (red circles, Fig. 2A). The wet season starts in late August to early September



250 during the early onset years, unlike the late-onset years when the onset delays until October (Table  
251 1). The rainforest also receives less rain ( $\sim 1$  mm/day) during the late-onset years (Fig. 2D).  
252 However, low cloud cover is higher during the late onset years after the 38<sup>th</sup> pentad as compared  
253 to the early-onset years (Fig. 2C).

254 Figures 3A-3D show the differences in the  $\delta T_s$  (shaded contours,) and the 650 hPa wind speed  
255 (arrows,  $\delta W_{\text{ind}}$ ) and wind direction over the domain between the early- and late-onset years from  
256 June to August. They show that the Congo rainforest is cooler by more than  $3^\circ\text{K}$  in June-August  
257 prior to the early-onsets. Such a cooling creates an early and stronger meridional temperature  
258 gradient throughout boreal summer before the wet season starts during the early onset years. As a  
259 result,  $\delta W_{\text{ind}}$  at 650 hPa is easterly as early as in June between  $8^\circ\text{S}$  - $16^\circ\text{S}$  (Fig. 3A). The wind  
260 speed difference between the early and late-onset years is significant ( $>3\text{ m/s}$ ) with respect to the  
261 climatological mean speed of  $\sim 7$  m/s (Adebiyi and Zuidema, 2016). The AEJ-S is known to form  
262 over the Southern hemisphere and gradually move towards the equator as the wet season  
263 approaches. In July (Fig 3B), the easterly  $\delta w_{\text{ind}}$  spreads over most of the domain.  $\delta W_{\text{ind}}$  is  
264 cyclonic in the Southern hemisphere in August (Fig. 3C) and over the Congo rainforest in  
265 September (Fig. 3D) during the early-onset years compared to the late-onset years. Consequently,  
266 Figure 5 shows that the southern hemisphere is more convergent during the early-onset years. As  
267 a result, high cloud cover (Fig. 2B) and precipitation (Fig. 2A) increase from August and wet  
268 season onsets as precipitation gradually increases. These findings suggest that stronger surface  
269 cooling and earlier formation of the AEJ-S lead to an earlier wet season onset.

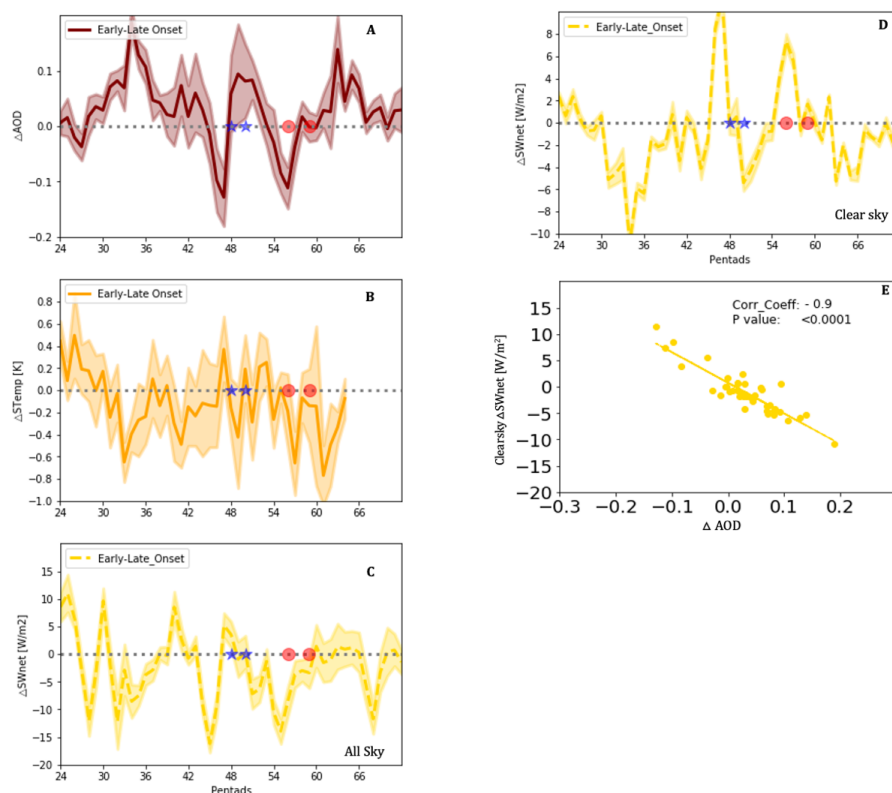


270

271 **Figure 3.** Map of differences in 2m skin temperature ( $\delta T_s$ , shaded contours) from AIRS and 650  
 272 hPa  $\delta$ wind (arrows) from ERA-interim between (A) 30<sup>th</sup>-36<sup>th</sup> pentads or June, (B) 36<sup>th</sup>-42<sup>nd</sup>  
 273 pentads or July, (C) 42<sup>nd</sup>-48<sup>th</sup> pentads or August, and (D) 48<sup>th</sup>-54<sup>th</sup> pentads or September  
 274 between three early-onset years (2007, 2011, and 2012) and three late-onset years (2003, 2006,  
 275 2010). Only the easterly winds are shown in (A) and (B) to show the location of AEJ-S.

276

277 Figure 4 shows the differences in various parameters related to the wet season onset between  
 278 the early- and late-onset years. Figure 4A shows that  $\delta$ AOD is positive during the early-onset  
 279 years from the 28<sup>th</sup> pentad (late May). The accumulation of aerosols in the early-onset years is  
 280 higher during the 30<sup>th</sup>-39<sup>th</sup> pentads and continues until the 45<sup>th</sup> pentad. The surface during the  
 281 early-onset years is cooler (Fig. 4B) than the late-onset years, with the strongest cooling  
 282 coinciding to (domain mean  $\delta T_s \sim -0.7^\circ$  K) with the higher  $\delta$ AOD during the 30-38<sup>th</sup> pentads in  
 283 June-mid July. All-sky  $\delta$ SW<sub>net</sub> is less (Fig. 4C) compared to the late-onset years. The reduced  
 284 all-sky  $\delta$ SW<sub>net</sub> can be attributed to higher  $\delta$ AOD (Fig. 4A) during the 30-38<sup>th</sup> pentads as cloud  
 285 cover difference is insignificant (Figs. 2B and C) during that time. The role of AOD on the  
 286 surface cooling is confirmed in Figure 4D, which shows that the clear-sky  $\delta$ SW<sub>net</sub> reaches up to -  
 287 10 W/m<sup>2</sup> during the 30-38<sup>th</sup> pentads. A strong negative correlation exists between the clear-sky



288

**Figure 4.** (A) Differences in MODIS AOD ( $\delta$ AOD) from the 24<sup>th</sup> (day 120) pentad to 72<sup>nd</sup> pentad (day 360), (B) As in A, but for  $\delta$ Ts from AIRS. Values up to 66<sup>th</sup> pentad are shown due to data unavailability in some days after the 66<sup>th</sup> pentad, (C) as in A, all-sky net downward shortwave energy difference at the surface ( $\delta$ SW<sub>net</sub>) from CERES, (D) As in A, but for clear-sky net downward shortwave energy difference at surface ( $\delta$ SW<sub>net</sub>) between the early and late-onset years from CERES. (E) Correlation between  $\delta$ AOD difference (in Fig. 3A) and clear-sky  $\delta$ SW<sub>net</sub> (in Fig. 3D) between the early and late-onset years at the surface.

296

297  $\delta$ SW<sub>net</sub> and  $\delta$ AOD during the 30-48 pentads ( $r=-0.9$ , Fig. 4E), suggesting that aerosols play a

298 significant role in reducing the SW<sub>net</sub> over the rainforest during the early-onset years. A lower all-

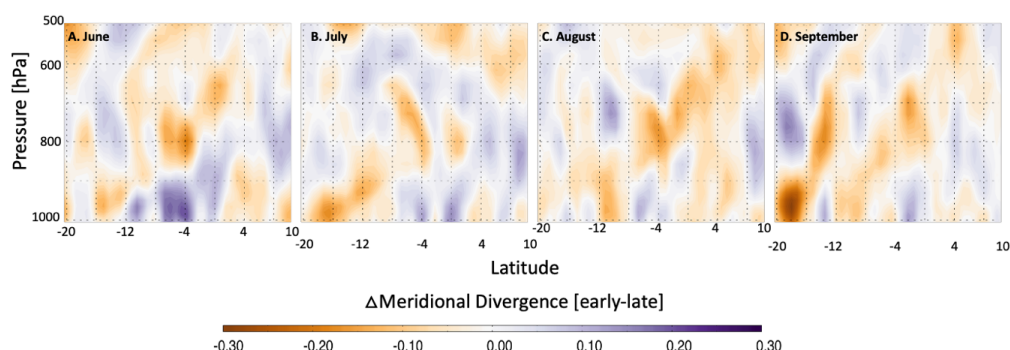
299 sky and clear-sky  $\delta$ SW<sub>net</sub> give rise to a lower  $\delta$ Ts. Hence, these results suggest that aerosols

300 have a strong impact on the timing and strength of the AEJ-S by reducing SW<sub>net</sub> at the surface





301 and Ts over the Congo rainforest. Such a cooling begins as early as in June and continues  
 302 throughout the summer during the early onset years.



303  
 304 **Figure 5.** Differences in the mean meridional divergence between 10°N to 20°S between 1000 hPa  
 305 to 500 hPa (Y axis) averaged over 12°E–32°E over between the early- and late-onset years during  
 306 (A) 30<sup>th</sup>–36<sup>th</sup> pentads or June, (B) 36<sup>th</sup>–42<sup>nd</sup> pentads or July, (C) 42<sup>nd</sup>–48<sup>th</sup> pentads or August, and  
 307 (D) 48<sup>th</sup>–54<sup>th</sup> pentads or September.

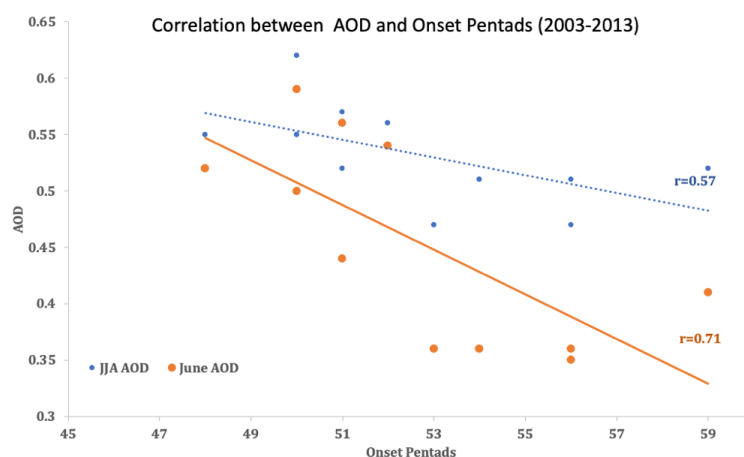
308

309 Several important changes in the cloud cover,  $SW_{net}$ , precipitation, and AOD occur after the  
 310 40<sup>th</sup> pentad during the early onset years. An early formation of AEJ-S and stronger easterly wind  
 311 makes the southern hemisphere more convergent (Figs. 5). The domain (5°N–10°S) experiences  
 312 a comparatively stronger convergence from August. Thus, high cloud cover (Fig. 2B) and  
 313 precipitation (Fig. 2A) increase between the 42<sup>nd</sup>–48<sup>th</sup> pentads during the early-onset years as  
 314 compared to late-onset years.  $\delta AOD$  also increases between the 40<sup>th</sup>–45<sup>th</sup> pentad (Fig. 4A). As a  
 315 result, clear-sky  $\delta SW_{net}$  reduces by 5 W/m<sup>2</sup> during 40–45 pentads (Fig. 4D), whereas all-sky  
 316  $\delta SW_{net}$  reduces by 18 W/m<sup>2</sup> during 43–47 pentads (Fig. 4C) because of higher high cloud cover  
 317 (Fig. 2B). Although clear-sky  $\delta SW_{net}$  increases by ~10 W/m<sup>2</sup> during 45–48 pentads as  $\delta AOD$   
 318 decreases due to higher precipitation and high/midhigh cloud cover, all-sky  $\delta SW_{net}$  only  
 319 increases by 5 W/m<sup>2</sup> after the 47<sup>th</sup> pentad. Hence,  $\delta Ts$  decreases by up to 3 K in August (Fig. 3C).  
 320 Mean  $\delta Ts$  over the domain decreases by 0.2–0.5 K (Fig. 4B) between 40–46<sup>th</sup> pentads. These





321 results point out that aerosol induced cooling in early boreal summer (June-mid July) leads to  
 322 higher cloud cover and precipitation in the late summer by influencing the timing and strength of  
 323 AEJ-S and associated convergence. Such changes in cloud cover in the late summer play a  
 324 significant role on the all-sky  $\delta SW_{net}$  and the domain Ts during the late summer (August). As a  
 325 result, the onset timing is highly correlated with the AOD over the domain. The correlation ( $r$ )  
 326 between the onset dates and the AOD averaged over June-August is 0.57 (Fig. 6). When June  
 327 AOD is correlated with the onset dates, correlation coefficient becomes even stronger ( $r = 0.7$ ).  
 328 These results indicate a close relationship between the dry period AOD and the wet season  
 329 timing over the Congo basin.

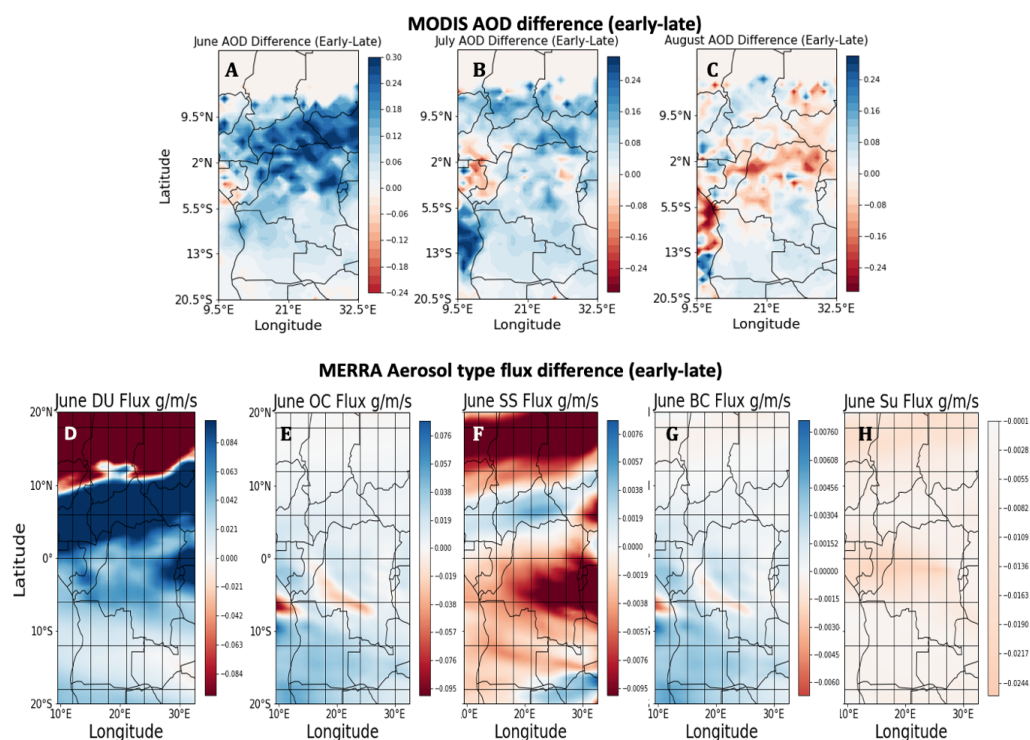


330  
 331 **Figure 6.** Correlation between the domain mean AOD between June-August and June with the  
 332 onset pentads.

333  
 334 Maps of  $\delta AOD$  from MODIS data are shown in Figs. 7A-C that confirm that the largest  
 335 difference in AOD is seen in June when  $\delta Ts$  is the highest and the AEJ-S begins (Fig.3A). We  
 336 further analyze the integrated aerosol mass flux datasets from MERRA2 reanalysis products to  
 337 understand what causes higher aerosol loading over the rainforest in June. The differences in

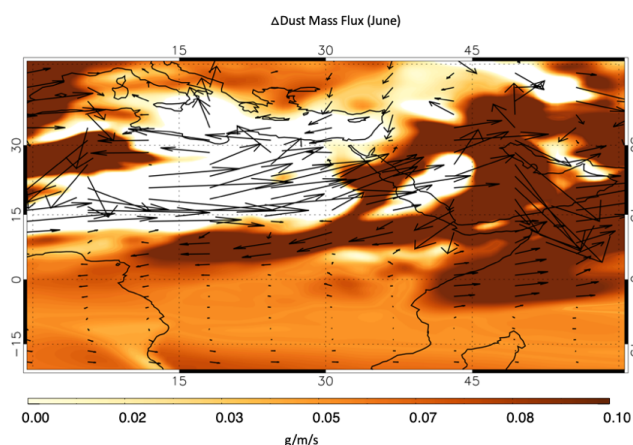


338 AOD between the early- and late-onset years is primarily due to the changes in the dust  
 339 concentrations (Fig. 7D) based on the MERRA2 integrated aerosol mass flux data sets (Randles  
 340 et al., 2017). The cause of the dust appears to be the long-range transport from the Eastern  
 341 Saharan Desert and the Arabian Desert (Fig. 8). Figure 8 suggests that the strength and location  
 342 of AEJ-N might play an important role in the aerosol transport from the Eastern Saharan Desert  
 343 and the Arabian Desert, thus on the aerosol concentration over the Congo rainforest and  
 344 associated early wet season onset.



345  
 346 **Figure 7.** Maps of MODIS AOD difference ( $\delta$ AOD) between the early and late-onset years in  
 347 (A) June, (B) July, and (C) August. Differences in MERRA2 aerosol flux for five different  
 348 species (D) dust, (E) organic carbon, (F) sea salt, (G), black carbon and (H) sulfate between the  
 349 early and late-onset years during June.

350



351

352 **Figure 8.** Map of differences in dust mass flux between the early and late-onset years from  
 353 MERRA2 data. Arrows show the direction of the dust mass flux difference.

354 Schematics in Figure 9 summarize the early- and late-onset mechanism and how aerosols play  
 355 a vital role in such differences. Higher aerosol concentrations during the early-onset years enhance  
 356 the reflection and scattering of the incoming solar energy in June. Thus, the rainforest receives a  
 357 lesser amount of downward shortwave energy. Consequently, the  $T_s$  decreases and driven by the  
 358 meridional temperature gradient between the rainforest and the Kalahari Desert, AEJ-S forms. In  
 359 August, the Kalahari Desert warms up as the Sun moves equatorward and the meridional  
 360 temperature gradient and AEJ-S strengthen. As a result, the equatorward convergence increases, a  
 361 stronger cyclonic circulation develops over the region, high cloud cover increases that lead to a  
 362 reduction in all-sky  $\delta SW_{net}$  and  $\delta T_s$ , and the wet season onsets in late August to early September.  
 363 In contrast, aerosol concentrations are less during the late-onset years. Hence, a higher amount of  
 364 solar energy reaches the surface and the rainforest  $T_s$  is higher than the early-onset years.  
 365 Therefore, the meridional temperature gradient is weaker or becomes negative in the Southern  
 366 Hemisphere with the Congo rainforest (Kalahari Desert) being warmer (cooler) during the boreal  
 367 summer (Austral winter, June-August). Consequently, the AEJ-S is delayed. In September, as the  
 368 Sun moves southward, the Kalahari Desert warms up. Compared to the early onset years, a weaker



meridional temperature gradient develops across the rainforest and the desert since the rainforest  
 Ts is higher (Fig. 3D) during the late-onset years. As a result, the AEJ-S is weaker. Not only is the  
 wet season delayed and the dry season lengthens, the Congo rainforest also receives lesser  
 precipitation.

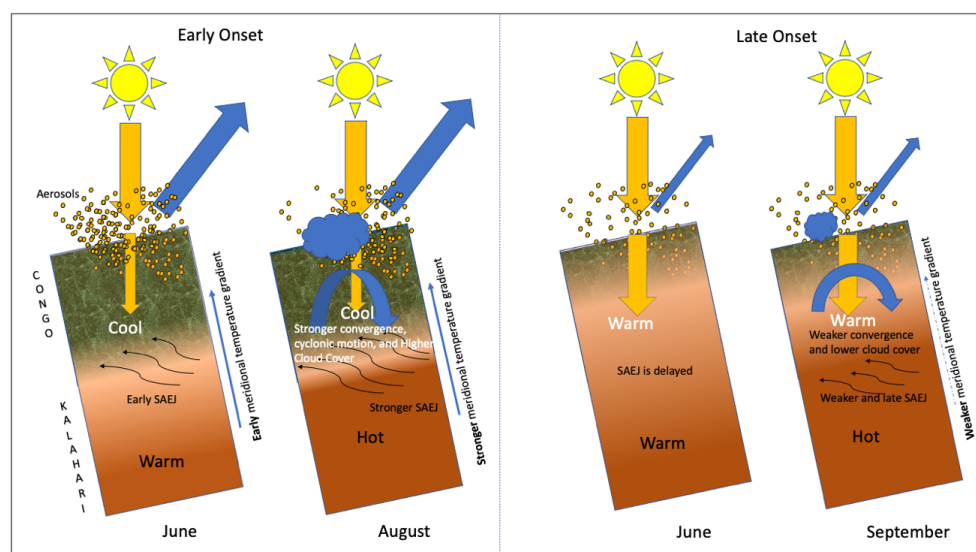


**Figure 9.** Schematics showing the early- (left) and late- (right) wet season onset mechanism.

#### 4. Conclusion

These above analysis results highlight the interconnections between the aerosols radiative  
 effect and the wet season onset timing by decreasing  $T_s$ , increasing meridional temperature  
 gradient, and influencing onset timing and strength of AEJ-S as well as associated convergence.  
 It is important to note that the meridional temperature gradient increases 2-3 months before the  
 wet season onset due to the surface cooling, which is caused by the aerosols dimming effect as  
 the Kalahari Desert is still cold during that time of the year. Because the main driver of the jet is  
 the meridional temperature gradient between the warm/dry Kalahari Desert and the moist Congo



rainforest, a reduction in the rainforest  $T_s$  (Figs. 3A-D and 4B) in the summer leads to an earlier and stronger AEJ-S during the early-onset years. Our results highlight an important connection between the reductions in the clear-sky  $\delta SW_{net}$  in early summer (June-mid July) due to aerosols, all-sky  $\delta SW_{net}$  in the late summer (August) due to a higher cloud cover, and early wet season onset.

These results indicate a plausible significant threat to the future of the Congo rainforest. Between 2003-2012, the regional temperature has increased by  $1.1^\circ\text{C}$  and the boreal summer dry season is increasing (Zhou et al., 2014). Thus, a projected increase in the global temperature anywhere between  $1.1^\circ$  to  $5.4^\circ\text{C}$  by 2100 (<https://www.climate.gov>) might be enough to offset a net mean rainforest cooling of  $\sim 1^\circ\text{C}$  required (Fig. 4B) for an early wet season onset over the region. This study identifies the role of aerosols on the wet season onset timing over the Congo Rainforest. Other factors, such as the location and strength of the AEJ-N and the tropical easterly jet might play an important role in the AOD variation (Fig. 8). Further analysis is required to understand the role of these jets and how their interannual variability in strength and location can impact the dust mass flux and wet season onset in the future, especially as the global temperature increases. Also, canopy cover reduction due to deforestation might affect the meridional temperature gradient and subsequently AEJ-S and the wet season onset. It is necessary to continue investigating the impacts of global warming, large-scale circulation change, land-use, and deforestation on the wet season onset over the Congo rainforest.

#### Author Contribution:

SC: design the research, analyzed data, wrote the paper.

JHJ: design the research, wrote the paper.

HS: design the research, wrote the paper.



407 RF: design the research, wrote the paper.

#### 408 **Competing Interests:**

409 The authors have no competing interests.

#### 410 **Acknowledgement**

411 This work was conducted at Jet Propulsion Laboratory, California Institute of Technology,  
412 under contract with NASA. This work was partly supported by NASA ROSES CCST Program.

#### 413 **Data and Code Availability**

414 All satellite data used in this study can be downloaded at the EOSDIS Distributed Active  
415 Archive Centers (DAACs) at <https://earthdata.nasa.gov/eosdis/daacs>. Please contact the  
416 corresponding author for any questions about how to download the data that are publicly available  
417 and codes written in IDL and Python.

#### 418 **References**

- 419 Adebisi, A. A. and Zuidema, P.: The role of the southern African easterly jet in modifying the  
420 southeast Atlantic aerosol and cloud environments, Q. J. R. Meteorol. Soc., doi:10.1002/qj.2765,  
421 2016.
- 422 Cook, K. H.: Generation of the African easterly jet and its role in determining West African  
423 precipitation, J. Clim., doi:10.1175/1520-0442(1999)012<1165:GOTAEJ>2.0.CO;2, 1999.
- 424 Cook, K. H. and Vizy, E. K.: The Congo Basin Walker circulation: dynamics and connections to  
425 precipitation, Clim. Dyn., doi:10.1007/s00382-015-2864-y, 2016.
- 426 Dezfuli, A. K. and Nicholson, S. E.: The relationship of rainfall variability in western equatorial  
427 africa to the tropical oceans and atmospheric circulation. Part II: The boreal autumn, J. Clim.,  
428 doi:10.1175/JCLI-D-11-00686.1, 2013.
- 429 Erfanian, A., Wang, G. and Fomenko, L.: Unprecedented drought over tropical South America in



- 430 2016: Significantly under-predicted by tropical SST, *Sci. Rep.*, doi:10.1038/s41598-017-05373-  
 431 2, 2017.
- 432 Fan, J., Wang, Y., Rosenfeld, D. and Liu, X.: Review of aerosol-cloud interactions: Mechanisms,  
 433 significance, and challenges, *J. Atmos. Sci.*, doi:10.1175/JAS-D-16-0037.1, 2016.
- 434 Gelaro, R., McCarty, W., Suárez, M. J., Todling, R., Molod, A., Takacs, L., Randles, C. A.,  
 435 Darmenov, A., Bosilovich, M. G., Reichle, R., Wargan, K., Coy, L., Cullather, R., Draper, C.,  
 436 Akella, S., Buchard, V., Conaty, A., da Silva, A. M., Gu, W., Kim, G.-K., Koster, R., Lucchesi,  
 437 R., Merkova, D., Nielsen, J. E., Partyka, G., Pawson, S., Putman, W., Rienecker, M., Schubert,  
 438 S. D., Sienkiewicz, M. and Zhao, B.: The Modern-Era Retrospective Analysis for Research and  
 439 Applications, Version 2 (MERRA-2), *J. Clim.*, 30(14), 5419–5454, doi:10.1175/JCLI-D-16-  
 440 0758.1, 2017.
- 441 Gueymard, C. A. and Yang, D.: Worldwide validation of CAMS and MERRA-2 reanalysis  
 442 aerosol optical depth products using 15 years of AERONET observations, *Atmos. Environ.*,  
 443 doi:10.1016/j.atmosenv.2019.117216, 2020.
- 444 Huang, L., Jiang, J. H., Tackett, J. L., Su, H. and Fu, R.: Seasonal and diurnal variations of  
 445 aerosol extinction profile and type distribution from CALIPSO 5-year observations, *J. Geophys.*  
 446 *Res. Atmos.*, doi:10.1002/jgrd.50407, 2013.
- 447 Jackson, B., Nicholson, S. E. and Klotter, D.: Mesoscale convective systems over western  
 448 equatorial Africa and their relationship to large-scale circulation, *Mon. Weather Rev.*,  
 449 doi:10.1175/2008MWR2525.1, 2009.
- 450 Jiang, Y., Zhou, L., Tucker, C. J., Raghavendra, A., Hua, W., Liu, Y. Y. and Joiner, J.:  
 451 Widespread increase of boreal summer dry season length over the Congo rainforest, *Nat. Clim.*  
 452 *Chang.*, doi:10.1038/s41558-019-0512-y, 2019.



- 453 Konzelmann, T., Cahoon, D. R. and Whitlock, C. H.: Impact of biomass burning in equatorial  
 454 Africa on the downward surface shortwave irradiance: Observations versus calculations, J.  
 455 Geophys. Res. Atmos., doi:10.1029/96jd01556, 1996.
- 456 Laurent, B., Marticorena, B., Bergametti, G., Léon, J. F. and Mahowald, N. M.: Modeling  
 457 mineral dust emissions from the Sahara desert using new surface properties and soil database, J.  
 458 Geophys. Res. Atmos., doi:10.1029/2007JD009484, 2008.
- 459 Lavaysse, C., Chaboureaud, J. P. and Flamant, C.: Dust impact on the west african heat low in  
 460 summertime, Q. J. R. Meteorol. Soc., doi:10.1002/qj.844, 2011.
- 461 Léon, J. F., Chazette, P., Pelon, J., Dulac, F. and Randriamiarisoa, H.: Aerosol direct radiative  
 462 impact over the INDOEX area based on passive and active remote sensing, J. Geophys. Res.  
 463 Atmos., doi:10.1029/2000JD000116, 2002.
- 464 Lewis, S. L., Brando, P. M., Phillips, O. L., Van Der Heijden, G. M. F. and Nepstad, D.: The  
 465 2010 Amazon drought, Science (80-. ), doi:10.1126/science.1200807, 2011.
- 466 Lewis, S. L., Sonké, B., Sunderland, T., Begne, S. K., Lopez-Gonzalez, G., van der Heijden, G.  
 467 M. F., Phillips, O. L., Affum-Baffoe, K., Baker, T. R., Banin, L., Bastin, J. F., Beekman, H.,  
 468 Boeckx, P., Bogaert, J., De Cannière, C., Chezeaux, E., Clark, C. J., Collins, M., Djagbletey, G.,  
 469 Djuikouo, M. N. K., Droissart, V., Doucet, J. L., Ewango, C. E. N., Fauset, S., Feldpausch, T. R.,  
 470 Foli, E. G., Gillet, J. F., Hamilton, A. C., Harris, D. J., Hart, T. B., de Haulleville, T., Hladik, A.,  
 471 Hufkens, K., Huygens, D., Jeanmart, P., Jeffery, K. J., Kearsley, E., Leal, M. E., Lloyd, J.,  
 472 Lovett, J. C., Makana, J. R., Malhi, Y., Marshall, A. R., Ojo, L., Peh, K. S. H., Pickavance, G.,  
 473 Poulsen, J. R., Reitsma, J. M., Sheil, D., Simo, M., Steppe, K., Taedoumg, H. E., Talbot, J.,  
 474 Taplin, J. R. D., Taylor, D., Thomas, S. C., Toirambe, B., Verbeeck, H., Vleminckx, J., White, L.  
 475 J. T., Willcock, S., Woell, H. and Zemagho, L.: Above-ground biomass and structure of 260





- 476 African tropical forests, *Philos. Trans. R. Soc. B Biol. Sci.*, doi:10.1098/rstb.2012.0295, 2013.
- 477 Li, W. and Fu, R.: Influence of cold air intrusions on the wet season onset over Amazonia, *J.*  
 478 *Clim.*, doi:10.1175/JCLI3614.1, 2006.
- 479 Loeb, N. G., Doelling, D. R., Wang, H., Su, W., Nguyen, C., Corbett, J. G., Liang, L., Mitrescu,  
 480 C., Rose, F. G. and Kato, S.: Clouds and the Earth's Radiant Energy System (CERES) Energy  
 481 Balanced and Filled (EBAF) top-of-atmosphere (TOA) edition-4.0 data product, *J. Clim.*,  
 482 doi:10.1175/JCLI-D-17-0208.1, 2018.
- 483 Malhi, Y. and Wright, J.: Spatial patterns and recent trends in the climate of tropical rainforest  
 484 regions, in *Philosophical Transactions of the Royal Society B: Biological Sciences.*, 2004.
- 485 Marcella, M. P. and Eltahir, E. A. B.: The role of mineral aerosols in shaping the regional  
 486 climate of West Africa, *J. Geophys. Res.*, doi:10.1002/2012JD019394, 2014.
- 487 Marengo, J. A., Nobre, C. A., Tomasella, J., Oyama, M. D., de Oliveira, G. S., de Oliveira, R.,  
 488 Camargo, H., Alves, L. M. and Brown, I. F.: The drought of Amazonia in 2005, *J. Clim.*,  
 489 doi:10.1175/2007JCLI1600.1, 2008.
- 490 Mayer, A. L. and Khalyani, A. H.: Grass trumps trees with fire, *Science* (80-. ),  
 491 doi:10.1126/science.1213908, 2011.
- 492 N'Datchoh, E. T., Diallo, I., Konaré, A., Silué, S., Ogunjobi, K. O., Diedhiou, A. and Doumbia,  
 493 M.: Dust induced changes on the West African summer monsoon features, *Int. J. Climatol.*,  
 494 38(1), 452–466, doi:10.1002/joc.5187, 2018.
- 495 Neupane, N.: The Congo basin zonal overturning circulation, *Adv. Atmos. Sci.*,  
 496 doi:10.1007/s00376-015-5190-8, 2016.
- 497 Nicholson, S. E.: The ITCZ and the seasonal cycle over equatorial Africa, *Bull. Am. Meteorol.*  
 498 *Soc.*, doi:10.1175/BAMS-D-16-0287.1, 2018.



- 499 Nicholson, S. E. and Dezfuli, A. K.: The relationship of rainfall variability in western equatorial  
 500 Africa to the tropical oceans and atmospheric circulation. Part I: The boreal spring, J. Clim.,  
 501 doi:10.1175/JCLI-D-11-00653.1, 2013.
- 502 Nicholson, S. E. and Grist, J. P.: The seasonal evolution of the atmospheric circulation over West  
 503 Africa and equatorial Africa, J. Clim., doi:10.1175/1520-  
 504 0442(2003)016<1013:TSEOTA>2.0.CO;2, 2003.
- 505 Randles, C. A., da Silva, A. M., Buchard, V., Colarco, P. R., Darmenov, A., Govindaraju, R.,  
 506 Smirnov, A., Holben, B., Ferrare, R., Hair, J., Shinozuka, Y. and Flynn, C. J.: The MERRA-2  
 507 aerosol reanalysis, 1980 onward. Part I: System description and data assimilation evaluation, J.  
 508 Clim., doi:10.1175/JCLI-D-16-0609.1, 2017.
- 509 Sitnov, S. A., Mokhov, I. I. and Likhoshesterova, A. A.: Exploring large-scale black-carbon air  
 510 pollution over Northern Eurasia in summer 2016 using MERRA-2 reanalysis data, Atmos. Res.,  
 511 doi:10.1016/j.atmosres.2019.104763, 2020.
- 512 Staver, A. C., Archibald, S. and Levin, S. A.: The global extent and determinants of savanna and  
 513 forest as alternative biome states, Science (80-. ), doi:10.1126/science.1210465, 2011.
- 514 Susskind, J., Blaisdell, J. M. and Iredell, L.: Improved methodology for surface and atmospheric  
 515 soundings, error estimates, and quality control procedures: the atmospheric infrared sounder  
 516 science team version-6 retrieval algorithm, J. Appl. Remote Sens., doi:10.1117/1.jrs.8.084994,  
 517 2014.
- 518 Tyukavina, A., Hansen, M. C., Potapov, P., Parker, D., Okpa, C., Stehman, S. V., Kommareddy,  
 519 I. and Turubanova, S.: Congo Basin forest loss dominated by increasing smallholder clearing,  
 520 Sci. Adv., doi:10.1126/sciadv.aat2993, 2018.
- 521 Vondou, D. A., Nzeukou, A., Lenouo, A. and Mkankam Kamga, F.: Seasonal variations in the



522 diurnal patterns of convection in Cameroon-Nigeria and their neighboring areas, Atmos. Sci.  
523 Lett., doi:10.1002/asl.297, 2010.

524 Whittleston, D., Nicholson, S. E., Schlosser, A. and Entekhabi, D.: Climate models lack jet-  
525 rainfall coupling over West Africa, J. Clim., doi:10.1175/JCLI-D-16-0579.1, 2017.

526 Wright, J. S., Fu, R., Worden, J. R., Chakraborty, S., Clinton, N. E., Risi, C., Sun, Y. and Yin,  
527 L.: Rainforest-initiated wet season onset over the southern Amazon, Proc. Natl. Acad. Sci. U. S.  
528 A., doi:10.1073/pnas.1621516114, 2017.

529 Xu, X., Wu, H., Yang, X. and Xie, L.: Distribution and transport characteristics of dust aerosol  
530 over Tibetan Plateau and Taklimakan Desert in China using MERRA-2 and CALIPSO data,  
531 Atmos. Environ., doi:10.1016/j.atmosenv.2020.117670, 2020.

532 Zhou, L., Tian, Y., Myneni, R. B., Ciais, P., Saatchi, S., Liu, Y. Y., Piao, S., Chen, H., Vermote,  
533 E. F., Song, C. and Hwang, T.: Widespread decline of Congo rainforest greenness in the past  
534 decade, Nature, doi:10.1038/nature13265, 2014.

535

536

537

538

539

540